RESEARCH ARTICLE | APRIL 07 2026

Stochastic behaviors of electrons through atom-vacancy defects in few atom-layer MoS_2-FETs and neuromorphic device application

K. Takaki; S. Furuichi ; M. Kosugi; H. Arisawa ; Y.-C. Lin ; T. Taniguchi ; K. Watanabe ; Y. Nonaka ; K. Suenaga ; E. Saitoh ; J. Haruyama

APL Electronic Devices 2, 026106 (2026)
https://doi.org/10.1063/5.0311764

APL Electronic Devices ARTICLE pubs.aip.org/aip/aed

Stochastic behaviors of electrons through atom-vacancy defects in few atom-layer MoS_2-FETs and neuromorphic device application

Cite as: APL Electron. Devices 2, 026106 (2026); doi: 10.1063/5.0311764
Submitted: 12 November 2025 • Accepted: 16 March 2026 •
Published Online: 7 April 2026 • Corrected: 13 April 2026

K. Takaki,[1] S. Furuichi,[2] M. Kosugi,[1] H. Arisawa,[3,4] Y.-C. Lin,[5] T. Taniguchi,[6] K. Watanabe,[7] Y. Nonaka,[1] K. Suenaga,[8] E. Saitoh,[3,4,9,10] and J. Haruyama[1,11,a)]

AFFILIATIONS

[1]Faculty of Science and Engineering, Aoyama Gakuin University, 5-10-1 Fuchinobe, Sagamihara, Kanagawa 252-5258, Japan
[2]Department of Electrical Engineering and Information Systems, The University of Tokyo, 4-6-1 Komaba, Meguro-ku, Tokyo 153-8505, Japan
[3]Department of Applied Physics, The University of Tokyo, 7-3-1 Hongo, Bunkyo-ku, Tokyo 113-8656, Japan
[4]RIKEN Center for Emergent Matter Science (CEMS), 2-1 Hirosawa, Wako, Saitama 351-0198, Japan
[5]National Institute of Advanced Industrial Science and Technology (AIST), Tsukuba 305-8565, Japan
[6]Research Center for Electronic and Optical Materials, National Institute for Materials Science, 1-1 Namiki, Tsukuba 305-0044, Japan
[7]Research Center for Materials Nanoarchitectonics, National Institute for Materials Science, 1-1 Namiki, Tsukuba 305-0044, Japan
[8]The Institute of Scientific and Industrial Research, The University of Osaka, Mihogaoka 8-1, Ibaraki, Osaka 567-0047, Japan
[9]Institute for AI and Beyond, The University of Tokyo, 7-3-1 Hongo, Bunkyo-ku, Tokyo 113-8656, Japan
[10]WPI Advanced Institute for Materials Research, Tohoku University, 2-1-1 Katahira, Aoba-ku, Sendai 980-8577, Japan
[11]Institute of Industrial Sciences, The University of Tokyo, 4-6-1 Komaba Meguro-ku, Tokyo 153-8505, Japan

[a)]**Author to whom correspondence should be addressed:** J-haru@ee.aoyama.ac.jp

ABSTRACT

Atom-vacancy defects existing in various materials yield numerous physical phenomena, hindering high performance in electronic and photonic devices in some cases. These become more significant in two-dimensional (2D) (atomically) thin van der Waals (vdW) layers. Meanwhile, their applications to novel devices have gathered significant attention. Neuromorphic (NM) computation, which directly mimics the probabilistic operation of the human brain through ion transport, is such an effective example due to its potential in developing power- and size-efficient artificial intelligence applications. While magnetic tunnel junctions currently represent the mainstream approach in NM computation, they require local magnetic fields, posing integration challenges with CMOS circuits. Here, we demonstrate that sigmoid circuits—representative NM circuits—can be operated only by leveraging low-frequency noises [noise currents (I_N) and power spectrum density (PSD)]—originating from the stochastic capture and emission of electrons through atom-vacancy defects—in few-atom-layer semiconductor molybdenum disulfide field-effect transistors. Modulating the back-gate voltage allows control of the magnitude of electrical hysteresis loops in the current and I_N (PSDs), thereby enabling and regulating the stochastic electron behaviors and emergence of the observed sigmoid operation. This work paves the way for the development of NM circuits through defect engineering in vdW 2D semiconductors, eliminating the need for magnetic fields.

I. INTRODUCTION

The physical behaviors derived from atom-vacancy defects and their application in highly efficient electronic and photonic devices are attracting considerable attention in two-dimensional (2D) (atomically) thin semiconductors [e.g., transition metal dichalcogenide (TMDC) family such as molybdenum disulfide (MoS_2)],[1–13] as even few atom-vacancy defects drastically alter those physical properties. Various types of atom-vacancy defects have been identified in these materials [e.g., sulfur (S) vacancies in MoS_2; Fig. 1(b)]. These defects result in various defect-derived mid-gap states with different activation energies (E_a) and electric behaviors.

Previously, we reported stochastic electronic properties, as well as dynamic behaviors such as low-frequency (LF) noise, arising from atom-vacancy defects in van der Waals (vdW) few-layer MoS_2 field-effect transistors (FETs).[1] We observed stochastic behaviors in large electrical hysteresis loops in the drain current (I_{sd}) vs back-gate voltage (V_{bg}) curves, applied from the backside of the substrate.[1] These findings indicate the presence of S-vacancy defect pairs localized near the junction interface of the MoS_2 flake and the SiO_2/Si substrate [similar to Figs. 1(a), 1(b), 1(e), and 1(f)]. Temperature (T)-dependent measurements and high-resolution transmission electron microscopy (HRTEM) analysis revealed that the hysteresis loops primarily originate from pairs of neighboring in-plane S vacancies [Figs. 1(a) and 1(b)] with an E_a of ~0.35 eV.

LF noise measurements [i.e., noise currents (I_N) and power spectral density (PSD)] of the samples have clarified the presence of stochastic capture and emission of charge carriers via S vacancy pairs.[1] PSD, obtained by Fourier transformation of I_N, directly reflects the physical behavior and characteristic parameters of these defects through LF noise analysis, as described by the following two equations reported in Ref. 1: Equation (1) comprises two Lorentzian components used to fit the measured PSD, whereas Eq. (2) is based on Shockley–Read–Hall (SRH) statistics and describes the defect-related parameters governing the stochastic capture and emission of charge carriers via defect states. The T-dependent term $f(T)$ in Eq. (2) is substituted for the frequency parameter f in Eq. (1), and the PSD fitting is performed using Eq. (1),

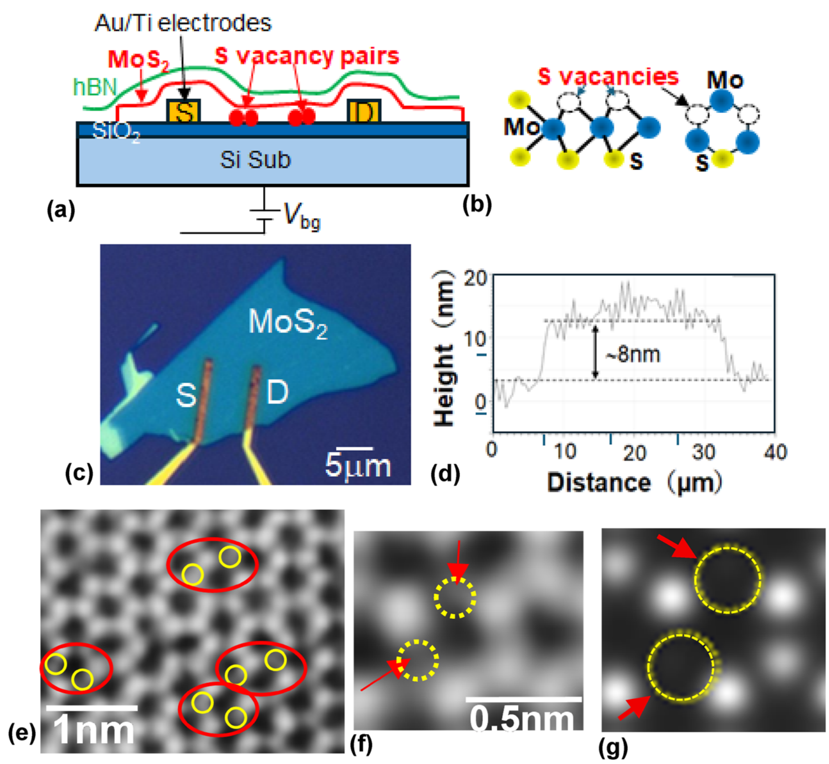

FIG. 1. (a) Schematic cross-sectional view of the MoS_2-FET with S vacancy-pair defects existing around the interface at the SiO_2 substrate. V_{sd} and V_{bg} are applied between the two electrodes (S–D) and from the sample backside, respectively. (b) Atomic structures of MoS_2, including S vacancies (left: cross section and right: top view). (c) An example of an optical microscope image showing a few-atom layer MoS_2 flake attached to pre-fabricated source (S) and drain (D) (Au/Ti) electrodes on a SiO_2/Si substrate (without a hBN cover layer, only for this image), fabricated using vdW mechanical exfoliation of bulk material with Scotch tape and PDMS sheet transfer technique. (d) Cross-sectional AFM image of (c). (e) Example of S-vacancy defect pairs (shown by red and yellow circles) observed using a high-resolution transmission electron microscope (HRTEM) around the MoS_2/SiO_2 interface, which corresponds to (b). (f) Zoomed-in and (g) simulated images of one S-defect pair in the upper part of (e) (indicated by red arrows and yellow circles).

$$S_I(f) = \frac{A_\alpha(I_c)I_c^2}{1+\left(\frac{f}{f_\alpha}\right)^2} + \frac{A_\beta(I_c)I_c^2}{1+\left(\frac{f}{f_\beta}\right)^2} + C, \qquad (1)$$

$$\tau(T) = \frac{1}{2\pi f(T)} = \frac{1}{\sigma \times \exp\left(\frac{-E}{kT}\right) \times N_T \times v}, \qquad (2)$$

where I_c is the fixed current, A_α and A_β denote the amplitudes of the Lorentzian components with characteristic corner frequencies f_α and f_β, respectively, while C represents a f-independent background accounting for the intrinsic noise floor of the measurement system, E is the activation energy of the defect level, N_T is the defect density, σ is the carrier capture cross section, and v is the electron velocity. Fitting the experimental data using this model provides detailed and quantitative information on the LF noise mechanisms.[1]

These processes generate large hysteresis loops, characterized by rapid transitions across narrow discrete states with a few-meV kinetic energy barriers, attributed to spin interactions in the parallel coupling of the two S vacancies.[1,3] The observed behavior suggested that coupled S vacancy pairs—exhibiting high uniformity and interacting with Mo atoms—created electronic states akin to those in quantum dots, despite the measurements encompassing multiple S-vacancy pairs at room T.[1]

The observed stochastic LF noises originating from S vacancy pairs could be highly suitable for probabilistic neuromorphic (NM) computation in artificial intelligence (AI), provided that the number, electronic states, and interactions of these defects can be controlled. Artificial neural networks (ANNs) with static neuron activation functions have recently emerged as the leading algorithm in AI. In contrast, NM computation, which directly mimics the probabilistic operation of the human brain, has garnered considerable attention for its potential in developing power- and size-efficient sensory processing, learning, and AI applications.[14–17]

A key element driving NM computation is the probabilistic operation—a robust classical mechanism fluctuating between 0 and 1 over time—resembling the stochastic behavior of the human brain through ion transport across films covering the brain's surface. However, because conventional CMOS circuits are not well-suited for stochastic operations, integrating quantum devices [e.g., magnetic tunnel junctions (MTJs) that leverage stochastic thermal fluctuations of electron spins] into CMOS-based NM circuits (e.g., sigmoid circuits with gradual changes between "0" and "1") has been challenging. While NM circuits employing MTJs have been widely developed and reported,[18–21] they require additional circuits to generate local magnetic fields, which may hinder their compatibility with CMOS technology. Therefore, the development of alternative stochastic (quantum) phenomena-based devices is highly anticipated to advance NM computation.

Moreover, although their operation is not inherently probabilistic, memristors—whose resistance varies according to the history of electrical signals applied to their two terminals—have attracted considerable attention for NM computation.[17,22,23] Because these resistance states can either persist for long durations or relax over short timescales, memristors can emulate the functions of electronic synapses and neurons in NM systems. Memristive behavior has been reported in a wide range of material platforms, including two-dimensional dichalcogenides, metal oxides and other ionic conductors, and halide perovskites. In particular, oxide-based systems such as WO_{3-x}-based nanoionic devices, oxygen-deficient $SrTiO_{3-x}$ (STO_x), and HfO_2 have been extensively studied. In these structures, ionic transport within the oxide layer between two metal electrodes gives rise to memristive operation.

In this study, we demonstrate that sigmoid operation representing NM circuits can be achieved by leveraging the stochastic LF noises [(I_N) and PSDs] generated by S vacancy pairs in few-layer MoS_2-FETs. It is revealed that modulating the V_{bg} alters the magnitude of the electrical hysteresis loops and I_N (PSDs), enabling the emergence and control of the probabilistic sigmoid operation.

II. RESULTS AND DISCUSSION

A. Sample and measurement-system preparation

In the present research, vdW-fabricated few-layer MoS_2 flakes are employed, with a current flow area of ~5 × 10 μm^2 between two Au/Ti electrodes [Figs. 1(a) and 1(c)]. Before exfoliation, the SiO_2/Si substrate surface is plasma-cleaned for 30 min under high vacuum. Few-layer MoS_2 flakes are mechanically exfoliated from bulk MoS_2 (purchased from HQ Graphene Co.) using Scotch tape and polydimethylsiloxane (PDMS) sheets, utilizing a 2D heterostructure transfer system (HQ Graphene Co.). The exfoliated flakes are subsequently transferred onto pre-fabricated Au/Ti electrodes on a SiO_2/Si substrate, leading to the emergence of S-vacancy defect pairs, as confirmed by HRTEM [Figs. 1(a), (b), and 1(e)–1(g)]. Moreover,

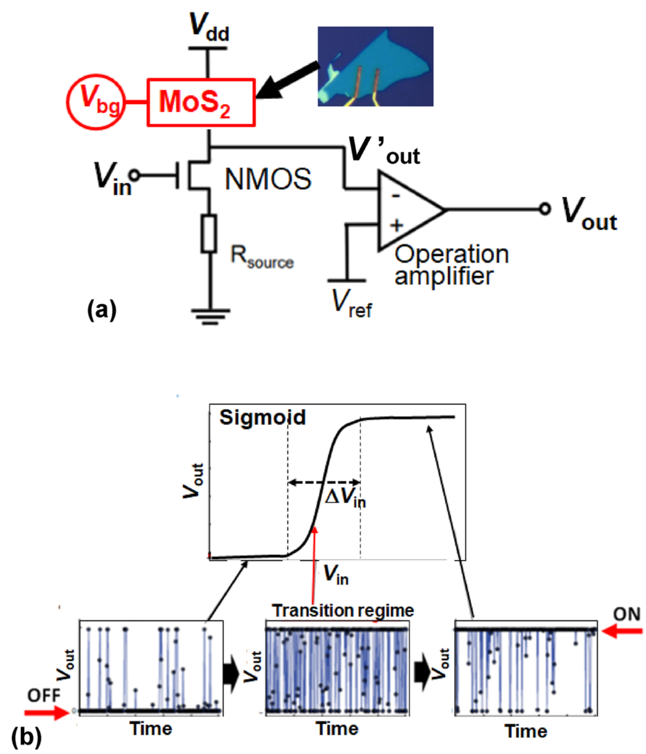

FIG. 2. (a) The sigmoid circuit used in the experiments, consisting of a MoS_2-FET shown in Fig. 1, an NMOS transistor, a source resistor (R_{source}), and an operational amplifier (op amp). (b) Schematic view for sigmoid operation based on (a) and stochastic behaviors of LF noises in MoS_2-FETs. Reprinted with permission from W. A. Borders, A. Z. Pervaiz, S. Fukami, K. Y. Camsari, H. Ohno, and S. Datta, Nature **573**, 390 (2019). Copyright Springer Nature.[18]

observation of the T and V_{bg} dependence of current (conductance) enabled precise determination of the E of S vacancy defects.[1] The extracted dominant E values of 0.2–0.35 eV are in good agreement with previously reported theoretical values characteristic of S-vacancy pairs. Consistent with the TEM observations, these results reconfirm that S-vacancy pairs are the primary contributors to the observed LF noise and hysteresis behavior.

The flake thickness (~8 nm) is confirmed via atomic force microscopy (AFM) [Fig. 1(d)] and Raman spectroscopy. After transfer, each sample is encapsulated with a high-quality hexagonal boron nitride (hBN) monolayer [Fig. 1(a)]. All fabrication steps are performed inside a glovebox under an Ar atmosphere. A back-gate electrode for applying V_{bg} is fabricated on the backside of the Si substrate [Fig. 1(c)], forming a FET structure. The LF noises (I_N and PSD) associated with S vacancy pairs are measured at room T, following the methodology described in Ref. 1.

In the present system, the physical parameters of the defects (e.g., N_T and E) in the MoS_2 flakes and the sigmoid operation can be connected through hysteresis loops and LF noises of the MoS_2-FETs, because these two behaviors arise from the same underlying mechanism—stochastic electron capture and emission via defect states—which follows SRH statistics [Eq. (2)] and is governed by parameters such as N_T and E, as described above. The magnitudes of the hysteresis loops and I_N are, therefore, proportional to the amplitude of these stochastic carrier capture and emission processes.

The sigmoid circuit employed in this study, which exploits the aforementioned stochastic behavior, consists of a MoS_2-FET, an NMOS transistor, a source resistor (R_{source}), and an op amp [Fig. 2(a)]. When the V_{in} value exceeds the NMOS V_{th}, the NMOS transistor turns on, electrically connecting the stochastic response of the MoS_2-FET to the ground, thereby setting the intermediate output voltage level before the op amp (V'_{out}) to 0 [lower-left panel of Fig. 2(b)]. Conversely, when V_{in} falls below V_{th}, the NMOS transistor turns off, disconnecting the MoS_2-FET from ground and instead connecting it to V_{dd}, setting the V'_{out} to 1 [lower-right panel of Fig. 2(b)]. It should be noticed that the op amp inverts the relationship between V_{in} and V'_{out}. As a result, V_{out} becomes 1 when $V_{in} > V_{th}$ and 0 when $V_{in} < V_{th}$ [lower-left and lower-right panels of Fig. 2(b)].

When the MoS_2 FET exhibits pronounced stochastic behavior, the transition of V_{out} between 0 and 1 occurs gradually across the transition V_{in} region (ΔV_{in}). As a result, the time-averaged V_{out} increases with V_{in}, yielding a characteristic sigmoid response with a large ΔV_{in} regime [Fig. 2(b), center panel].

This operation has been optimized by varying R_{source} (0.1–10 KΩ), V_{ref} (0.001–0.1 V), and the NMOS device parameters. The combination that produced the most pronounced sigmoid behavior has been selected for the measurements.

Readout/circuit noise has been excluded using Savitzky–Golay (SG) filtering applied to the measured LF noises, as described in Ref. 1. This filtering has significantly reduced such parasitic noise components. Moreover, the amplitude of I_N and the PSD in the low f regime increased markedly with increasing fixed S–D current of the MoS_2-FETs, whereas no such dependence was confirmed when carbon resistors were used instead. These results strongly indicate that the observed behaviors here are not associated with conventional circuit noise.

B. Sample basic properties; V_{bg}-dependent hysteresis curves, I_N, and PSDs

Figure 3 presents the I_{sd} vs V_{sd} (a) and I_{sd} vs V_{bg} characteristics [(b) and (c)] measured at room temperature, as fundamental electrical properties of MoS_2-FETs shown in Fig. 1. For light irradiation in (a), LED light (AS ONE, AS3000; the wavelength with a peak around 600 nm and a width between 480 and 780 nm, power 30 000 Lx) is used. Consistent with our previous findings in Ref. 1,

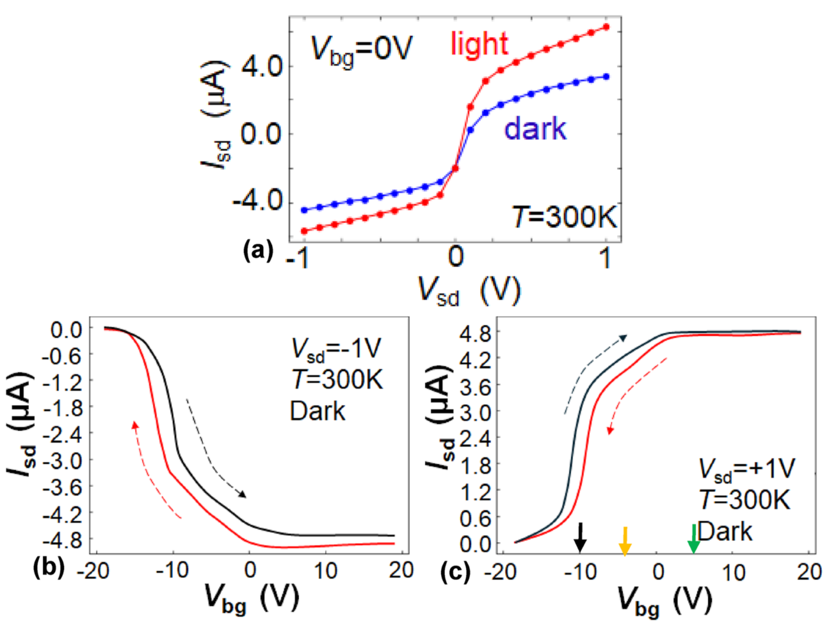

FIG. 3. (a) I_{sd} vs V_{sd} curves measured at V_{bg} = 0 V under dark and light ambient, and [(b) and (c)] I_{sd} vs V_{bg} curves measured at V_{sd} = −1 V (b) and +1 V (c) at room temperature, as fundamental electric properties of MoS_2-FET shown in Fig. 1(a). LED light (AS ONE, AS3000; the wavelength with a peak around 600 nm and a width between 480 and 780 nm, power 30 000 Lx) is used for irradiation in (a). Black (V_{bg} = −10 V) and green (V_{bg} = +5 V) solid arrows shown on the x-axis in (c) represent the V_{bg} positions used for the measurements in Figs. 4 and 5.

pronounced hysteresis is observed only in the I_{sd} vs V_{bg} curves (i.e., in the negative V_{bg} region at a fixed V_{sd} of +1 V) when V_{bg} is swept [Figs. 3(b) and 3(c)]. As discussed earlier,[1–3] this hysteresis behavior is attributed to the difference in the stochastic capture and emission of charge carriers triggered by sweeping V_{bg} along different V directions between $+V_{bg}$ and $-V_{bg}$ regions, through S vacancy pairs at the MoS_2 flake/substrate interface, because V_{bg} is applied from the backside of the MoS_2 flake [Figs. 1(a) and 1(b)].

Although several alternative sources of LF noise may be considered (e.g., surface SiO_2/interface traps, interface states at Au/Ti electrode contacts, and carrier mobility fluctuations), the present results indicate that their contributions are minor. When V_{sd} is applied, I_{sd} flows through these surface regions and contact interfaces; if S-vacancy defects in these areas are dominant, a much larger hysteresis would be expected in the I_{sd}–V_{sd} characteristics. Such behavior was not observed. In addition, mobility fluctuations of carriers transported between the S and D electrodes would primarily depend on V_{sd}. The pronounced dependence on the V_{bg}, therefore, supports the conclusion that S-vacancy pairs located near the MoS_2 flake/substrate interface are the primary origin of the observed LF noise.

Figures 4(a) and 4(b) exhibit an example of LF noise (I_N) observed at V_{bg} = +5 V, where Δ_{hys} is minimal [shown by the blue arrow in Fig. 3(c)], and at V_{bg} = −10 V, where Δ_{hys} is maximal [shown by the red arrow in Fig. 3(c)], respectively, when a constant I_{sd} (I_c) of 1 μA is flowed between the source and drain electrodes at room temperature. The results indicate that the magnitude of I_N (ΔI_N) at V_{bg} = −10 V is significantly larger than ΔI_N at V_{bg} = +5 V. PSDs transformed from these I_N are shown in Figs. 4(c) and 4(d), based on Ref. 1. It is evident that the magnitude of the PSD of (c) measured at V_{bg} = −10 V is two-order smaller than that of (d) measured at V_{bg} = +5 V. These are qualitatively consistent with our previous results,[1] which clarified that the I_N and PSD magnitude are proportional to the Δ_{hys} because both the current hysteresis loops and LF noises originate from the stochastic capture and emission of charge carriers via the S vacancy pairs, which highly depend on applied V_{bg}.

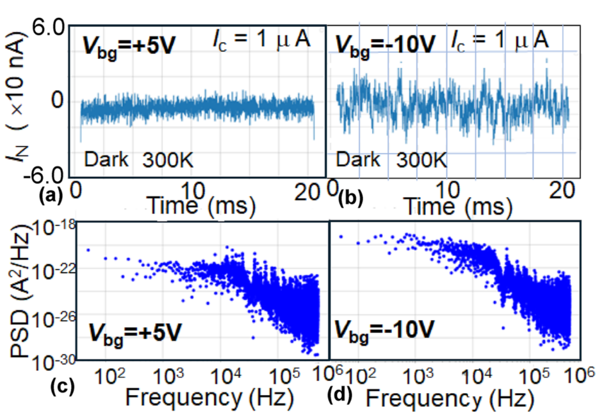

FIG. 4. [(a) and (b)] Example of LF noise current (I_N) observed at S–D electrodes [Figs. 1(a) and 2] at V_{bg} = +5 V (a) and −10 V (b) [in Fig. 3(c)] under a constant I_{sd} = 1 μA. [(c) and (d)] PSDs Fourier-transformed from [(a) and (b)], respectively.

As mentioned above, the current hysteresis loops are attributed to the different ratios of these carrier capture and emission of electrons caused by the different V_{bg}-sweep direction between $\pm V_{bg}$ regions. Meanwhile, LF noises arise from the thermal emission of electrons and their capture when the constant I_{sd} flows along the current channel of MoS_2-FETs, depending on the constant V_{bg} for the different hysteresis-loop positions. The PSDs in Fig. 4(d) indicate the narrow discrete energy states, E ~3 meV, formed in the S vacancy pairs and defect density, N_T ~10^{11}/cm^2, based on Refs. 1 and 3.

C. Sigmoid operation controllable by V_{bg}

The MoS_2-FET is introduced into the sigmoid circuit shown in Fig. 2, and the presence of sigmoid characteristics is examined by modulating Δ_{hys} through variations in the applied V_{bg}. Figures 4(b) and 5(a) display the time-dependent V_{out} response as a function of V_{in}, measured using an oscilloscope, at V_{bg} = +5 V and V_{bg} = −10 V in Figs. 3(c)–3(e), respectively. The results show a clear difference between the two conditions. At V_{bg} = +5 V [Fig. 5(a)], V_{out} exhibits an abrupt jump from low (0) to high (1) between V_{in} = 1.38 and 1.39 V. In contrast, at V_{bg} = −10 V [Fig. 5(b)], V_{out} transition is more gradual between V_{in} = 1.28 and 1.38 V, implying an expanded transition region for V_{in} (ΔV_{in}). These results imply a strong correlation among Δ_{hys}, ΔI_N (PSDs), and ΔV_{in} via the stochastic capture and emission of charge carriers through the S-vacancy pairs. With the small ΔI_N (PSDs) at V_{bg} = +5 V, V_{out} directly transits from low (0) to high (1) just according to the changes in V_{in} in the circuit shown in Fig. 2. In contrast, the large ΔI_N (PSDs) at V_{bg} = −10 V leads to the appearance of the intermediate region (ΔV_{in}) due to the stochastic electron capture and emission through S-vacancy defect pairs.

Representative V_{in}–V_{out} characteristics obtained at three different V_{bg} values (i.e., different ΔI_N) for three different samples with similar E and ΔI_N are presented in Fig. 5(c), distinguished by three different symbols and colors. For instance, for the sample corresponding to Figs. 5(a) and 5(b) (circle symbols), V_{out} switches abruptly (digitally) at V_{in} = 1.38 V for V_{bg} = +5 V (green symbol) without a noticeable transition ΔV_{in} region. As V_{bg} decreases to −5 V (blue symbol), where Δ_{hys} is slightly larger, V_{out} transition becomes more gradual (analog) between $V_{in} \approx$ 1.45 V and $V_{in} \approx$ 1.52 V. At V_{bg} = −10 V (black symbol), a clear transition region ΔV_{in} emerges between V_{in} = 1.28 and 1.4 V, yielding a pronounced sigmoid characteristic. These trends are consistent with those observed in Figs. 4(a) and 4(b). The other two samples exhibit nearly identical behavior when ΔI_N is tuned to comparable values by V_{bg} (i.e., within the same color group). Figure 5(e) shows a representative example of the high reproducibility of ΔV_{in} for the black circles shown in Fig. 5(c), indicating a narrow distribution of ΔV_{in} within 0.04 V for five repeated measurements.

Figure 5(d) presents the dependence of ΔV_{in} on ΔI_N for the three samples, including the results presented in Fig. 5(c) (surrounded by three dashed squares). As ΔI_N increases, ΔV_{in} expands in all three samples, particularly from ΔI_N of ~20 nA. The small ΔI_N samples show ΔV_{in} ~ 0. This trend reconfirms a strong correlation between the stochastic capture and emission of charge carriers through S vacancy defect pairs, which generate the ΔI_N, and the observed sigmoid characteristics, ΔV_{in}, via Δ_{hys}.

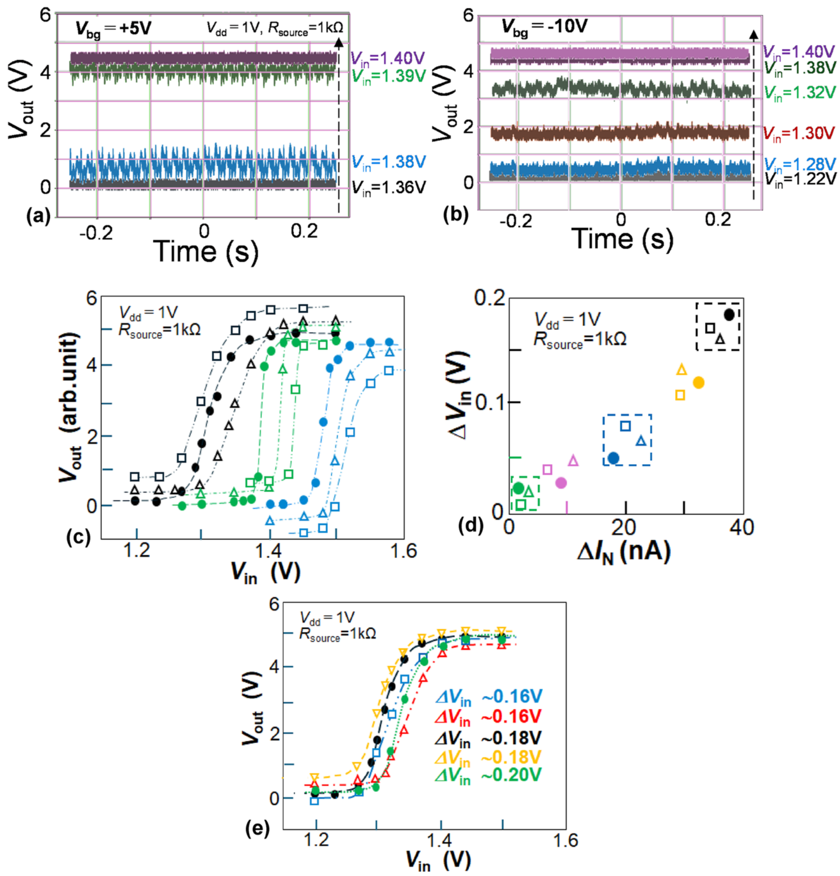

FIG. 5. Time-dependent V_{out} response as a function of V_{in} in Fig. 2-sigmoid circuit introducing Fig. 3-sample, measured using an oscilloscope, (a) at V_{bg} = +5 V [with the minima Δ_{hys} shown by the blue arrow in Fig. 3(c) and corresponding to Figs. 4(a) and 4(c)] and (b) at V_{bg} = −10 V [with the maximum Δ_{hys} shown by the red arrow in Fig. 3(c) and corresponding to Figs. 4(b) and 4(d)]. (c) Representative V_{in}–V_{out} characteristics for three different samples (distinguished by symbol type) measured at three different V_{bg} values (distinguished by different colors), including the sample shown in [(a) and (b)] (shown by circle symbols). For each sample, the V_{bg} values, which show similar I_N levels among samples, have been selected. The V_{bg} values for the circle symbols correspond to the arrows of the same color indicated on the x-axis of Fig. 3(c). (d) Dependence of the transition V_{in} width (ΔV_{in}) on ΔI_N for three different samples (i.e., shown by different symbols), including the results shown in (c). Different symbol colors correspond to different ΔI_N (V_{bg}) values. The symbols' data surrounded by the three dashed squares are shown in (c). (e) Results of five-time repeated measurements near the wide ΔV_{in} regime of the black-circle-symbol sample in [(c) and (d)], showing the narrow ΔV_{in} distribution within 0.04 V.

As mentioned above, the magnitude of LF noises (ΔI_N and PSD) increases with an increase in Δ_{hys}. This is because Δ_{hys} is governed by the amplitude of stochastic electron capture and emission through S-vacancy defect pairs, which differently responds to the different V_{bg}-sweep direction between the applied $\pm V_{bg}$, while these stochastic capture and emission processes are also thermally caused at room T, depending on the constant V_{bg} values during noise measurements. As the constant V_{bg} values are modulated for an increase in Δ_{hys}, these processes intensify, leading to an increase in LF noises. Consequently, the enhanced LF noises (ΔI_N), arising from the stochastic electron capture and emission through S vacancy pairs, evidently result in an increase in ΔV_{in} and thus allow the emergence of the observed sigmoid operation.

III. CONCLUSION

In conclusion, we have presented that the sigmoid circuits can be operated by utilizing LF noises—originating from the stochastic capture and emission of electrons through S-vacancy defect pairs—in few-atom-layer MoS_2-FETs. Modulating V_{bg} has allowed control of the Δ_{hys}, ΔI_N (PSDs), and appearance of the sigmoid operation. This work opens the doors for the development of NM circuits through defect engineering in vdW 2D semiconductors, without usage of magnetic fields.

ACKNOWLEDGMENTS

We thank T. Kikkawa, S. Maruyama, T. Kohno, T. Ando, E. Tsymbal, J. J. Palacios, R. Wu, and P. Kim for their technical contributions, fruitful discussions, and encouragement. The work at the Aoyama Gakuin University was partly supported by the Aoyama Gakuin University Research Institute grant program for the creation of innovative research. The work at the University of Tokyo was partly supported by JST-CREST (Grant Nos. JPMJCR20C1 and JPMJCR20T2), Grant-in-Aid for Scientific Research (Grant Nos. JP19H05600 and JP24K01326), and Grant-in-Aid for Transformative Research Areas (Grant Nos. JP22H05114 and JP24H02231) from JSPS KAKENHI, MEXT Initiative to Establish Next-generation Novel Integrated Circuits Centers (X-NICS) (Grant No. JPJ011438), Japan, and Sumitomo Chemical. K.W. and T.T. acknowledge support from the JSPS KAKENHI (Grant Nos. 20H00354, 21H05233, and 23H02052) and World Premier International Research Center Initiative (WPI), MEXT, Japan.

AUTHOR DECLARATIONS

Conflict of Interest

The authors have no conflicts to disclose.

Author Contributions

K. Takaki: Data curation (lead). **S. Furuichi**: Supervision (equal). **M. Kosugi**: Data curation (equal). **H. Arisawa**: Supervision (equal). **Y.-C. Lin**: Data curation (equal); Investigation (equal). **T. Taniguchi**: Resources (equal). **K. Watanabe**: Resources (equal). **Y. Nonaka**: Investigation (equal). **K. Suenaga**: Supervision (equal). **E. Saitoh**: Supervision (equal). **J. Haruyama**: Conceptualization (lead); Supervision (lead); Writing – original draft (equal).

DATA AVAILABILITY

The data that support the findings of this study are available from the corresponding author upon reasonable request.

REFERENCES

[1] M. Kosugi *et al.*, ACS Appl. Mater. Interfaces **16**(46), 64190 (2024).
[2] M. Kosugi *et al.*, AIP Adv. **12**, 105210 (2022).
[3] Y. Nonaka, K. Takaki, Y. Kobayashi, and J. Haruyama, AIP Adv. **15**, 045202 (2025).
[4] Y. Katagiri *et al.*, Nano Lett. **6**, 3788 (2016).
[5] Y. Nagamine *et al.*, Appl. Phys. Lett. **117**, 043101 (2020).
[6] S. H. Song *et al.*, Nat. Commun. **8**, 2121 (2017).
[7] Y. Zhao *et al.*, Nat. Commun. **14**, 44 (2023).
[8] J. Y. Kim, Ł. Gelczuk, M. P. Polak, D. Hlushchenko, D. Morgan, R. Kudrawiec, and I. Szlufarska, npj 2D Mater. Appl. **6**, 75 (2022).
[9] A. Hötger *et al.*, npj 2D Mater. Appl. **7**, 30 (2023).
[10] E. Mitterreiter *et al.*, Nat. Commun. **12**, 3822 (2021).
[11] V. K. Sangwan, H. N. Arnold, D. Jariwala, T. J. Marks, L. J. Lauhon, and M. C. Hersam, Nano Lett. **13**, 4351 (2013).
[12] J. Frunie *et al.*, Nano Lett. **25**(14), 5836 (2025).
[13] T. W. Tang *et al.*, ACS Nano **19**, 8509 (2025).
[14] J. Puebla, J. Kim, K. Kondou, and Y. Otani, Commun. Mater. **1**, 24 (2020).
[15] A. Hoffmann, S. Ramanathan, J. Grollier *et al.*, APL Mater. **10**, 070904 (2022).
[16] R. Xu *et al.*, Nano Lett. **19**, 2411 (2019).
[17] E. Chicca and G. Indiveri, Appl. Phys. Lett. **116**, 120501 (2020).
[18] W. A. Borders, A. Z. Pervaiz, S. Fukami, K. Y. Camsari, H. Ohno, and S. Datta, Nature **573**, 390 (2019).
[19] J. Torrejon *et al.*, Nature **547**, 428 (2017).
[20] M. Romera *et al.*, Nature **563**, 230 (2018).
[21] N. Locatelli, V. Cros, and J. Grollier, Nat. Mater. **13**, 11 (2014).
[22] I. Boybat, M. L. Gallo, T. Moraitis *et al.*, Nat. Commun. **9**, 2514 (2018).
[23] S. Pi, C. Li, H. Jiang, W. Xia, H. Xin, J. J. Yang, and Q. Xia, Nat. Nanotechnol. **14**, 35 (2019).